CORE
Metadata, citation and similar papers at core.a
Provided by NERC Open Research Archive

JOURNAL OF GEOPHYSICAL RESEARCH, VOL. 114, C04009, doi:10.1029/2008JC005147, 2009

Damping of Tropical Instability Waves caused by the action of surface currents on stress

R. Justin Small,[1,2] Kelvin J. Richards,[1,3] Shang-Ping Xie,[1,4] Pierre Dutrieux,[3] and Toru Miyama[5]

Received 4 October 2008; revised 24 December 2008; accepted 10 February 2009; published 25 April 2009.

[1] Ocean eddies and fronts affect surface stress via two mechanisms: (1) ocean surface currents altering the relative motion between air and sea and, hence, the stress fields and (2) ocean sea surface temperature (SST) gradients forcing changes in stability and near-surface winds. In this paper, we quantify the first effect and how it impacts Tropical Instability Waves (TIW) in the eastern Pacific. High-resolution satellite data and a regional coupled model are used to distinguish between stress changes due to the surface currents and those due to the changes in stability and near-surface winds. It is found that both mechanisms affect the surface stress curl, but they do so at different latitudes, allowing for their effect on Ekman pumping to be distinguished. The Ekman pumping due to the surface current effect alone, leads to significant damping of the TIWs. In terms of the eddy kinetic energy, the inclusion of surface current in the stress leads to decay with an e-folding time comparable with the period of the TIWs. It is, thus, an important damping mechanism to be included in ocean and coupled ocean-atmosphere models.

Citation: Small, R. J., K. J. Richards, S.-P. Xie, P. Dutrieux, and T. Miyama (2009), Damping of Tropical Instability Waves caused by the action of surface currents on stress, *J. Geophys. Res.*, *114*, C04009, doi:10.1029/2008JC005147.

1. Introduction

[2] Recent studies have identified two dominant means by which ocean mesoscale features (such as fronts and eddies) affect the surface stress. Firstly, the surface stress and its curl field, and hence the Ekman pumping, are modified not just by winds, but also by the presence of ocean currents. Ocean currents give rise to a relative motion between atmosphere and ocean, and hence modify the surface stress [*Bye*, 1986]. In this paper we treat this simply as a change in relative velocity of the interface, and we do not consider more complex modulation of the stress due to wave-current interaction [*Johannessen et al.*, 1996].

[3] Secondly, surface stress is modified by the SST gradients associated with ocean features, as a result of a combination of the change in wind speed, and the change in stability as airflows across different SST regimes [as reviewed by *Xie*, 2004; *Chelton et al.*, 2004; *Small et al.*, 2008]. A common feature of these studies is that the low level wind speeds and hence the magnitude of the stress above ocean mesoscale features tend to be larger over warm SST and weaker over cool SST. Changes in the surface stress due to these mechanisms can also be accompanied by changes in the gradients of the stress, which are important to upper ocean circulation.

[4] The aim of this paper is to investigate the relative effect of the ocean surface current and atmospheric boundary layer adjustment on the stress fields over Tropical Instability Waves (TIWs) in the eastern Pacific, and to deduce the impact this has on the ocean eddies. TIWs are important to the heat budget of the Equatorial Cold Tongue [*Jochum et al.*, 2004; *Jochum and Murtugudde*, 2006; *Menkes et al.*, 2006; *Dutrieux et al.*, 2008] as well as being associated with significant biological activity [*Yoder et al.*, 1994; *Menkes et al.*, 2002]. They are also believed to rectify onto interannual SST and precipitation variability [*Jochum et al.*, 2007; *Zhang and Busalacchi*, 2008].

[5] Note that as the atmospheric response to TIWs has already been well studied and quantified, as reviewed in section 2.2, this allows the current effect to be better distinguished, and the feedback to be better understood. We use a regional coupled model and satellite measurements of surface stress, SST, and surface height to perform the investigation. The paper is structured as follows. In section 2, a background is given on the two mechanisms of stress adjustment. Section 3 describes the data, the model and the methods. Section 4 quantifies the reduction in eddy kinetic energy (EKE) and the change of decay rates of the TIWs when surface currents act on the stress fields. Section 5 then explains in more detail how the damping takes place via Ekman pumping, and distinguishes this from the effects of the changes in surface stability and near-surface winds. This is followed by a Discussion of how the feedback mechanisms affect the heat

[1]International Pacific Research Center, University of Hawaii, Honolulu, Hawaii, USA.
[2]Naval Research Laboratory, Stennis Space Center, Mississippi, USA.
[3]Department of Oceanography, School of Ocean and Earth Science and Technology, University of Hawaii, Honolulu, Hawaii, USA.
[4]Department of Meteorology, School of Ocean and Earth Science and Technology, University of Hawaii, Honolulu, Hawaii, USA.
[5]Frontier Research for Global Change, Japan Agency for Marine-Earth Science and Technology, Yokohama, Japan.

Copyright 2009 by the American Geophysical Union.
0148-0227/09/2008JC005147$09.00

budget of the eastern Equatorial Pacific Ocean, and we finish with Conclusions. The major finding of the study is that the impact of surface stress modulations due to surface currents on ocean eddies is significant both in observations and model: this has been known for the mean current field, but previously has been shown only theoretically for eddies [*Dewar and Flierl*, 1987].

2. Background

2.1. Stress Modification by Surface Ocean Currents: The "Understress"

[6] *Bye* [1986] studied the impact of surface currents on the stress by the change in the relative motion and termed it "understress": this term will be used in this paper henceforth. He noted that the air-sea interface exerts a drag on both the atmosphere (via wind stress) and the ocean (via understress). *Bye* [1986] derived the total surface stress in bulk flux form as

$$\underline{\tau} = \underline{\tau_a} - \underline{\tau_o}$$
$$\underline{\tau_a} = C\underline{U}_{10} \;\; \underline{\tau_o} = C\underline{U}_C, \tag{1a}$$

where

$$C = \frac{\rho_a}{(1+\varepsilon)^2} C_D |\underline{U}_{10} - \underline{U}_C|. \tag{1b}$$

Here $\underline{U}_{10}$ is the 10 m wind vector, $\underline{U}_C$ the surface ocean current, C_D is the 10 m drag coefficient, and ρ_a is air density. ε^2 is the ratio of the product of density and drag coefficient in air to that in seawater. In most applications the ratio is assumed negligible so that

$$\underline{\tau} = \rho_a C_D |\underline{U}_{10} - \underline{U}_C| (\underline{U}_{10} - \underline{U}_C) = \rho_a C_D |\underline{U}_s| \underline{U}_s, \tag{2}$$

where $\underline{U}_s = \underline{U}_{10} - \underline{U}_c$ is the relative surface motion. The fact that the ocean current does appear in the surface stress has been noted by several investigators using satellite scatterometer measurements [*Kelly et al.*, 2001; *Cornillon and Park*, 2001; *Chelton et al.*, 2004; *Park et al.*, 2006].

[7] Various analytical and numerical models have been used to study the impact of the "understress" on the equatorial ocean currents and the cold tongue [e.g., *Pacanowski*, 1987; *Luo et al.*, 2005]. Less attention has paid to the effect on mesoscale eddies, with the exception of the studies discussed next.

[8] The impact of understress on ocean eddies can be understood by considering the Ekman pumping w_E, given by

$$w_E = \frac{1}{\rho_0} \nabla x \frac{\underline{\tau}}{f}, \tag{3}$$

where f is the Coriolis acceleration, $\underline{\tau}$ is the surface stress vector defined above, and ρ_0 is an average water density. *Dewar and Flierl* [1987] considered the effect of the full formulation of stress on ocean eddies (including surface ocean current $\underline{U}_c$ in equation (2)) in a quasigeostrophic framework on an f plane ($f = f_0$). Linearizing ($\underline{U}_{10} - \underline{U}_c$) about the atmospheric wind, when the background wind is zonal, the additional Ekman pumping due to the understress effect is approximately given by

$$w'_E \cong \frac{\rho_a}{\rho_0} C_D U_{10} \frac{(2u_{cy} - v_{cx})}{f_0}, \tag{4a}$$

where $\underline{U}_c = (u_c, v_c)$ and subscripts x and y denote differentiation. For an axisymmetric vortex, with $v_{cx} = -u_{cy}$, the relative vorticity $\xi = -2u_{cy}$, so that expression (4a) can be rewritten

$$w'_E \cong \frac{\rho_a}{\rho_0} C_D U_{10} \frac{3\xi}{2f_0}. \tag{4b}$$

[9] This extra term results in a relaxation of the thermocline and is analogous to bottom friction: it is referred to by Dewar and Flierl as "top drag." Numerical experiments showed that the dissipation of the eddy due to this top drag was over three times more effective than from a more standard biharmonic interior friction.

[10] *Martin and Richards* [2001] investigated the impact of this effect on an anticyclonic eddy in the North Atlantic, and estimated Ekman pumping anomalies up to 1 mday^{-1}. This made a significant contribution to the vertical flux of nutrients, an argument supported by *in situ* measurements by *McGillicuddy et al.* [2007]. It is worth remarking that whereas cyclonic and anticyclonic mode 1 eddies are damped by the top-drag effect, the near surface vertical motion in the mode-water (mode 2 "lens") eddies by *McGillicuddy et al.* [2007] are enhanced. This is because the latter has upward motion at the top of the pycnocline, whereas the geostrophic currents are determined by the depression at the bottom of the thermocline. The top drag causes upward motion to enhance the doming of the upper pycnocline and to transport nutrients vertically.

[11] *Seo et al.* [2007] showed that the perturbation surface currents of TIWs can alter the surface stress estimate over the TIW region by ±20%. *Polito et al.* [2001] computed the Ekman pumping associated with TIWs and displayed a Hövmoller diagram of the properties averaged between 1.5°N and 3.5°N. By comparing the SSH anomaly and the Ekman pumping, and finding them in phase, they deduced that the Ekman pumping was due to the surface currents of TIWs impacting on the surface stress. As suggested by *Dewar and Flierl* [1987], the TIW "vortex" is feeling a drag at the sea surface.

2.2. Stress Modification by Ocean Eddies due to Atmospheric Boundary Layer Adjustment to SST

[12] Several investigators have found modification of low level winds and surface stress over Tropical Instability Waves (TIWs) [*Hayes et al.*, 1989; *Xie et al.*, 1998; *Liu et al.*, 2000; *Hashizume et al.*, 2001; *Chelton et al.*, 2001]. In addition to the already noted increase of stress over warmer water, *Chelton et al.* [2001] described the consequences of this for the stress gradient fields. Positive wind stress curl tends to be generated when the wind blows along the SST isotherms of the northern TIW front, due to the shear between the higher speeds to the right and lower speeds to the left of the air parcel. They find an observed linear relationship between wind stress curl and the crosswind component of SST

gradient. In addition, the wind stress divergence is found to be linearly related to the alongwind component of SST gradient, as winds are often found to diverge as they cross SST fronts. *Chelton et al.* [2004] and *O'Neill et al.* [2005] extended this work to find similar relationships in most of the eddy-rich regions of the World's oceans. Following *Seo et al.* [2007] we will refer to this mechanism of stress modulation as the SST-wind feedback.

[13] A few studies have looked at the effect of these modifications of stress on the underlying ocean, in particular via the Ekman pumping. The consequent modification of sea surface height (SSH) by Ekman pumping is seen in the linear vorticity equation under long wave approximation: [e.g., *White and Annis*, 2003]. The relevant terms here are

$$\frac{\partial \eta}{\partial t} - c_R \frac{\partial \eta}{\partial x} = -\frac{\rho'}{\rho_0} w_E + \ldots, \tag{5}$$

where ρ' is the potential density difference between the upper ocean and the interior ocean, and ρ_0 is an average water density. Hence positive (negative) Ekman pumping velocity acts to decrease (increase) the SSHA. *White and Annis* [2003] found that this would affect the translational motion of a warm anticyclonic eddy in the northern hemisphere. Under background westerly winds, the positive (negative) curl found north (south) of the eddy acted to reduce (increase) the SSH anomaly (SSHA) via the Ekman pumping, thus leading to an equatorward motion.

[14] The coupled modeling study by *Seo et al.* [2007] showed that the atmospheric wind response to SST anomalies in TIWs is negatively correlated with the surface currents. This indicated that TIWs are damped by the overlying atmospheric wind response. In an analysis of the eddy kinetic energy (EKE) equation, they estimated this effect to be roughly 10% of the barotropic conversion source term in the tropical Atlantic Ocean.

[15] *Spall* [2007] investigated the effect of SST induced wind stress curl anomalies on baroclinic ocean eddies using an oceanic quasigeostrophic model with the Ekman pumping determined to be a function of the SST gradient. For the case of wind blowing from warm to cold water, he found that the growth rate of the instabilities could be enhanced relative to the Eady problem for uncoupled flow. *Spall* [2007] also found that strong stratification, weaker oceanic jets (less advection), and low latitudes favor stronger coupling. Thus it may be expected that the process would be important for Tropical Instability Waves near the equator. Here the airflow is from cold to warm in which case the expectation is that there will be a damping effect. Indeed, in an earlier study *Pezzi et al.* [2004], who used a similar parameterization of wind stress anomalies, note a decrease in SST variability in TIWs when the coupling was switched on.

[16] In the present study we extend the results by *Polito et al.* [2001], *Chelton et al.* [2001], *Pezzi et al.* [2004] and *Seo et al.* [2007] to distinguish and quantify the SST-wind coupling mechanism and the understress mechanism and their effects on TIWs.

3. Data and Methods

[17] In this paper satellite observations will be used to diagnose the combined effects of SST-wind feedback and understress on the TIWs. However, these data cannot easily be used to distinguish between these feedback mechanisms, and therefore we also employ a regional ocean-atmosphere model to perform sensitivity studies.

3.1. Satellite Data

[18] To study the observed relationship between surface stress, SST, and surface currents we utilize three complementary satellite data sets. SST was gathered from the Tropical Rainfall Measuring Mission (TRMM) Microwave Imager (TMI). TMI data is not affected by clouds and hence has a significant advantage over infrared radiometers in regions of large cloud cover [*Wentz et al.*, 2000]. For near-surface wind and stress estimates, we use the QuikSCAT SeaWinds scatterometer. QuikSCAT normalized cross-section is calibrated against 10 m neutral wind vectors deduced from buoy measurements (as discussed for NSCAT by *Wentz and Smith* [1999]). In order to convert to surface stress we use the *Large and Pond* [1981] formalism. For both SST and winds we use the daily 3-day running mean product from Remote Sensing Systems (www.ssmi.com), processed on a 0.25° grid. Sea level data is gathered in the form of combined TOPEX/POSEIDON and European Remote Sensing satellite sea level anomaly from Centre National d'Etudes Spatiales (CNES) Archiving, Validation and Interpretation of Satellite Oceanographic data (AVISO [*Ducet et al.*, 2000]), from October 1992, on a 0.25° grid, every 10 days. The anomaly is defined relative to a 7-year time mean for 1993–1999.

3.2. Regional Coupled Model

[19] The IPRC Regional Ocean Atmosphere Model (IROAM) is run for the eastern Pacific domain [*Xie et al.*, 2007]. It comprises a regional atmospheric model [*Wang*, 2001; *Wang et al.*, 2004] and the MOM2 ocean model [*Pacanowski and Griffies*, 2000]. The sigma coordinate atmospheric model has 28 sigma levels, 8 of which are in the lower 1000 km to better resolve the boundary layer. The z coordinate ocean model has 30 levels, 20 of which are in the upper 400 m. Vertical mixing in the ocean is based on the *Pacanowski and Philander* [1981] scheme, and lateral mixing is governed by a constant Laplacian eddy viscosity coefficient of 200 $m^2\ s^{-1}$.

[20] A ½°, co-located grid is employed for the ocean T, S and tracer points and the atmospheric unstaggered grid. *Xie et al.* [2007, their Figure 1] show the domain of the complete model system. The fully coupled ocean–atmosphere part of the model covers the Pacific Ocean from 150°W eastward to the American coastline, and from 30°S to 30°N. In this interactive domain, the coupling occurs once per day, and fluxes are derived from the *Fairall et al.* [2003] bulk formulae using daily mean values of the SST (and surface currents for the understress case) from the ocean model and near–surface temperature and humidity from the atmospheric model. The ocean model is initialized by setting the temperature and salinity equal to *Levitus* [1982] January climatology and velocity set to zero. It is spun up from 1991 to 1996 using basin wide forcing from NCEP/NCAR reanalysis [*Kalnay et al.*, 1996], then the interactive coupling is switched on from 1996 to 2003. Further details and an overview of the model performance can be found in the work of *Xie et al.* [2007]. Lateral boundary conditions and initial

conditions of the atmospheric model are obtained from the NCEP/NCAR reanalysis.

[21] The coupled model is modified to include the understress effect in a similar fashion to that described by *Song et al.* [2006]. First the relative surface motion $\underline{U}_s = \underline{U}_{10} - \underline{U}_c$ is found using the uppermost layer ocean current and the lowest layer atmospheric velocity. This is used in the calculation of the bulk surface fluxes (see equation (2)). These bulk fluxes (stress, heat flux) are then used as boundary forcing for the ocean model. For the atmospheric model, the lowest layer momentum equation includes the effect of the ocean current in the vertical diffusion [*Song et al.*, 2006, their equations (6) and (7)]. This approach is equivalent to the fully coupled run by *Luo et al.* [2005].

3.3. Methods and Model Experiments

[22] In order to highlight the effect of the TIWs, we high pass filter the data longitudinally, by removing a 12° running average, and then linearly regress onto a variable at a fixed point where the variance is high (e.g., filtered SST at 2°N, 120°W), following *Hashizume et al.* [2001]. This technique effectively highlights the effect of TIWs on the atmosphere and the stress fields. The linear regressions presented here are done using daily data in order to derive smooth, well-sampled fields. For the satellite altimetry, the 10 day gridded SSHA data was linearly interpolated in time to a daily resolution. Although the altimetry data significantly undersamples the TIWs (which have periods of 17–30 days), the results are still useful when used in conjunction with well-resolved model data which was compiled into daily averages. Further, the linear regression uses a long time series of data where many measurements are taken of the different phases of TIWs (i.e. from a number of different TIW vortices); in that sense, it provides a reasonably well-sampled data set.

[23] For consistency between observations and model, we use 10 m neutral equivalent wind $\underline{U}_{10N}$ instead of 10 m wind $\underline{U}_{10}$. Here a modification of equation (2) needs to be considered. In the absence of currents

$$\underline{\tau} = \rho C_{DN} \left|\underline{U}_{10N}\right| \left(\underline{U}_{10N}\right),$$

where $C_{DN} = C_D|\underline{U}_{10}|^2/|\underline{U}_{10N}|^2$ is the neutral drag coefficient. C_{DN} is independent of stability and is a function only of the 10 m neutral wind speed for a motionless surface. When currents are considered, the drag coefficient becomes a function of the change in speed between the surface and 10 m. However, as the Large and Pond drag coefficient is constant (1.2×10^{-3}) for wind speed changes within the range 4 to 11 m s^{-1} (including most of the range of winds considered in this study, see section 3.1), we will assume also that the small (<1 m s^{-1}) adjustments to the wind made by assuming neutral stratification and/or by adding ocean currents do not change the drag coefficient.

[24] Three main model simulations are presented to investigate the sensitivity of the model system to the feedbacks of interest. A control run contains full coupling, including the understress effect, and is referred to as Experiment 1 (Exp. 1). A second simulation was performed identical to the control except that the understress effect was switched off (Exp. 2). In addition, an atmosphere-only run was performed for comparison with coupled simulations, termed Exp. 3, which uses TMI daily SST (a 3-day running average), as a surface boundary condition. The latter run has the advantage of having observed SST at the surface, allowing a direct evaluation of the SST-wind feedback effect against observations.

4. Dynamic Variability of the Tropical Instability Waves

[25] An overall comparison of the regional coupled model and observations is presented in *Xie et al.* [2007]. Here we concentrate on the TIW activity and begin by comparing the EKE and the SSH variability in the coupled model runs and in observations.

4.1. Eddy Kinetic Energy and Sea Surface Height Variability

[26] The level of TIW activity can be characterized by a suitably defined eddy kinetic energy (EKE). We write the ocean velocity $\underline{u} = \underline{U} + \underline{u}'$, where $\underline{U}$ is taken to be the velocity field associated with the large scale flow field and $\underline{u}'$ an eddy component. For this analysis we use the spatial high pass filter described in section 3.3 to define the eddy component [*Hashizume et al.*, 2001]. (When using this spatial filter, the time mean of $\partial\underline{u}'/\partial t$ is not necessarily zero, but in practice it is near zero.) The EKE is given by $1/2\rho_0(u'^2 + v'^2)$, and is computed from one year of data, 1 May 2000 to 30 April 2001, which includes one full TIW "season". A depth average of the EKE is then performed to a depth of 95 m, which is close to the depth of the core of the EUC in the eastern Pacific.

[27] The EKE in the model case with understress (Exp. 1, Figure 1a) reaches a maximum in the longitude range 135°W to 120°W and between the equator and 2°N. When averaged in longitude between 140°W to 110°W (Figure 2), the peak value for Exp. 1 is nearly 66 J m^{-3}, close to the equator. When the understress is removed (Exp. 2, Figures 1b and 2), the EKE is increased, to around 100 J m^{-3}, about 1½ times the Exp.1 value.

[28] As this stage it would be useful to compare with observations, but estimates of EKE from observations are mostly confined to close to the Equator [e.g., *Qiao and Weisburg*, 1998] where the TAO ADCP are located, or along a particular longitudinal section (e.g., *Luther and Johnson* [1990] computed an EKE which peaked at 2°N at around 75 J m^{-3} at 70 m depth and averaged over 3 longitudes between 150°W and 160°W, estimated from their Figures 5 and 9). However, individual velocity component covariances were computed by *Baturin and Niiler* [1997] from a large (nearly 2000 member) sample of Lagrangian drifters in the tropical Pacific Ocean. They found that at 15 m depth, the meridional eddy velocity covariance $\rho_0(v'^2)$ reached a maximum of approximately 75 J m^{-3} close to the equator and at 120°W, and over 125 J m^{-3} at around 3°N (derived from their Plate 4c). These values are comparable to those of total EKE found in the model, but a more quantitative comparison is not undertaken due to the different time periods and/or longitudes used in the *Luther and Johnson* [1990] and *Baturin and Niiler* [1997] study.

[29] A better quantitative comparison can be made by analyzing the sea surface height anomaly measured from satellite directly and that from the model data. (This has the added advantage that the data can be filtered in the same way

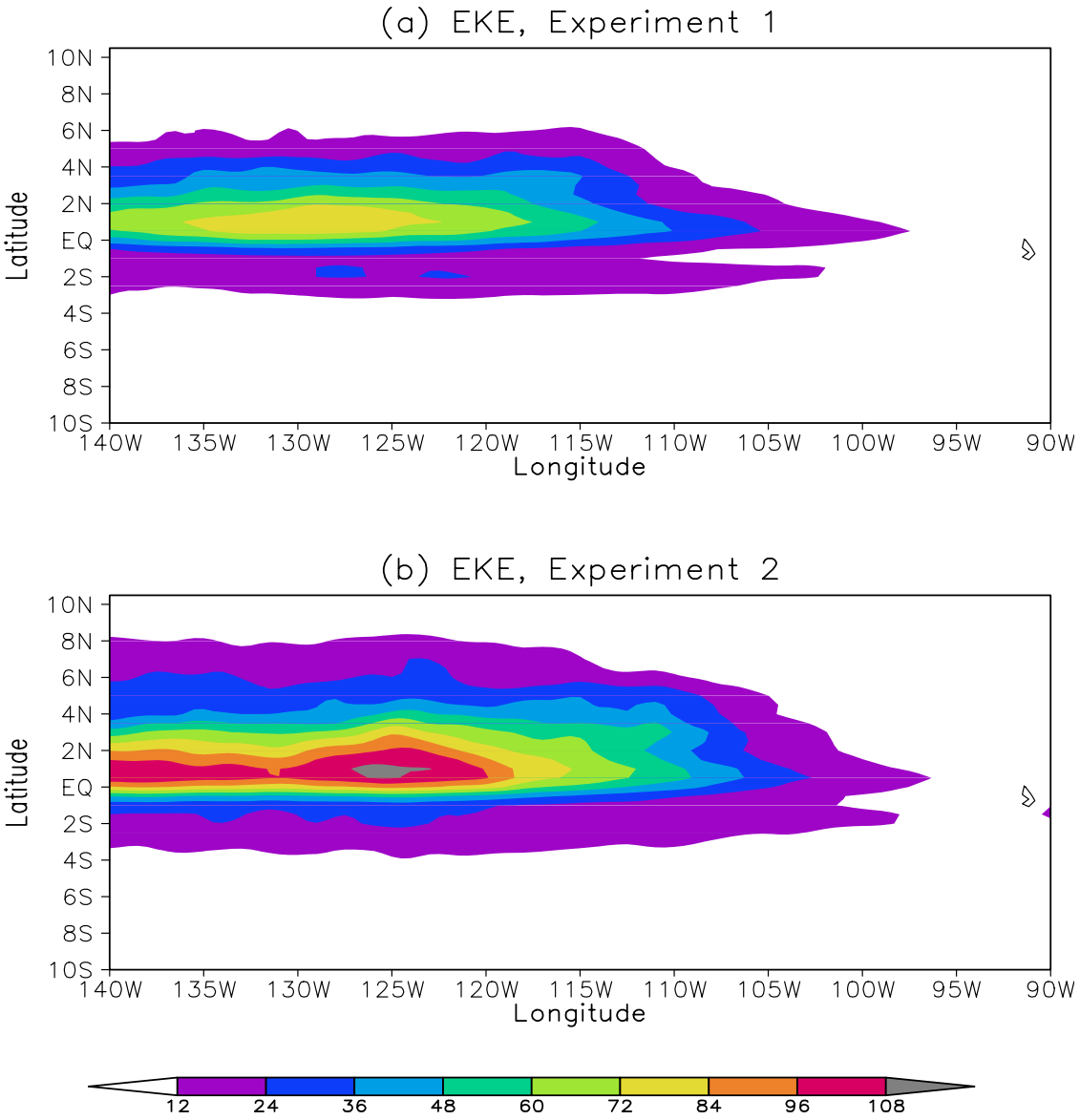

Figure 1. EKE (Jm^{-3}), depth averaged from the surface to 95m. (a) Experiment 1 and (b) Experiment 2.

as the model to highlight the TIWs.) For this analysis, the SSH data is filtered spatially as before to highlight the TIWs, and for the model data the time mean is removed (this has already been done in the altimetry product), to derive SSHA. The root mean square (RMS) of SSHA was computed from 3 years of data (1998–2000). The observed SSHA is greatest around 6°N and between 140°W and 130°W in these years, with maximum amplitude between 6 and 7 cm (Figure 3a). In Exp. 1, the maximum RMS of SSHA is weaker than observed (less than 5 cm), and located further east and slightly south of the observed maximum (Figure 3b). When the understress is removed (Exp. 2), the maximum RMS of SSHA is actually closer to that observed (Figure 3c).

[30] Two important points arise from Figures 1 to 3. Firstly, the eddy activity is significantly reduced when understress is included. This may arise due to the direct damping of the eddy field by the "top drag" effect [*Dewar and Flierl*, 1987; *Polito et al.*, 2001], or indirectly by reducing the mean current shear [*Pacanowski*, 1987] and hence the level of instability and energy conversions which leads to eddy activity. This is discussed further below. Secondly, it is noteworthy that the observed SSH variability appears to be comparable to or larger than the model run with no understress, and significantly greater than the case with understress. This point is interesting in itself, but the comparison with observations should not be used to say whether Exp. 1 or Exp. 2 is more "skillful" than the other, because of the strong sensitivities of the model to other, more tunable parameters, in particular the horizontal, constant Laplacian eddy viscosity, and the vertical eddy viscosity, which are less physically based than the understress effect. Instead, it suggests that the amount of momentum mixing in the model may be too low, because of deficiencies of the mixing scheme.

4.2. Eddy Kinetic Energy Budget

[31] A common method of analyzing the generation and dissipation of TIWs is to compute the eddy kinetic energy (EKE) budget [e.g., *Luther and Johnson*, 1990; *Masina et al.*,

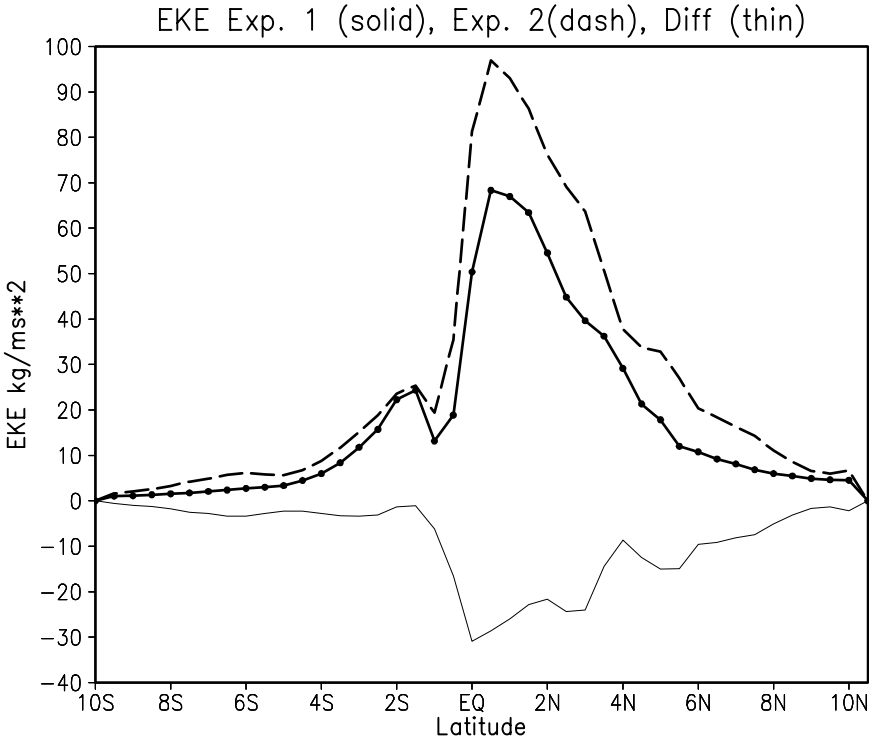

Figure 2. EKE (J m^{-3}, equivalently kg m^{-1} s^{-2}), depth averaged to 95 m then averaged between longitudes 140°–110°W. Thick solid line, Experiment 1; dashed line, Experiment 2; thin solid line, Experiment 1–Experiment 2.

1999]. The EKE budget shows the relative importance of different mechanisms of energy transfer (e.g., via baroclinic or barotropic instabilities or diffusion). Previous studies have suggested that TIWs generate from barotropic instability occurring on the meridional shear between the northern branch of the South Equatorial Current (SECN) and the North Equatorial Countercurrent (NECC [*Philander*, 1978]), or on the meridional shear between the Equatorial Undercurrent (EUC) and SECN [*Luther and Johnson*, 1990; *Qiao and Weisburg*, 1998; *Masina et al.*, 1999], or from baroclinic instability [*Cox*, 1980; *Luther and Johnson*, 1990]. The latter is at least partly due to the presence of the northern SST front [*McCreary and Yu*, 1992; *Masina et al.*, 1999]. The debate over which mechanism is most important is complicated by the proposed existence of two distinct types of waves, one near the equator and one further north possibly associated with the SST front [see *Cox*, 1980; *Luther and Johnson*, 1990; *McCreary and Yu*, 1992; *Kennan and Flament*, 2000; *Lyman et al.*, 2007, for more details].

[32] It is not the purpose here to add to these discussions of the generation mechanisms for TIWs, but it is important to compute the generation terms of the EKE equation in order to better understand the counteracting role of understress. However, the EKE budget is sometimes difficult to interpret as it represents a balanced state after the various mechanisms have all played their part. In order to detect the tendency that would occur due to a particular mechanism alone, we also propose below a simple modification of the EKE terms.

[33] The standard EKE terms for the ocean model have been stated by, e.g., *Luther and Johnson* [1990] and *Masina et al.* [1999], while *Baturin and Niiler* [1997] and *Seo et al.* [2007] also include the term which involves work done by surface stress on the eddies. Of interest here are the conversion terms, and the stress work term, which may be written in depth-averaged form as

$$\begin{aligned} BT &= -\rho_0 \left\langle \underline{u'} \cdot \left(\underline{u'} \cdot \frac{\partial \underline{U}}{\partial x}, \underline{u'} \cdot \frac{\partial \underline{U}}{\partial y} \right) \right\rangle . \\ BC &= -g \langle \rho' w' \rangle \\ S &= \frac{\left(\underline{u_c}' \cdot \underline{\tau'} \right)}{h}, \end{aligned} \tag{6}$$

where BC is the baroclinic conversion, BT is the barotropic conversion and S is the stress-feedback damping term due to the interaction of the part of the stress modified by the TIWs with the TIW surface current field, the term of interest here. Here the angled brackets denote a depth average to depth h, $\underline{u_c}$ is the ocean surface velocity, $\underline{u'}$ and $\underline{U}$ are the depth dependent ocean eddy and large scale current respectively, and τ is the surface stress.

[34] The reason why the stress-work term provides a damping is illustrated in Figure 4, taken from Experiment 1 with full coupling and understress. The filtered SST (color), surface stress (black arrows) and surface current (white arrows) are all regressed onto filtered SST at 2°N, 120°W. As noted by *Seo et al.* [2007], the surface stress anomalies oppose the current anomalies over much, but not all, of the domain shown. This is due to both the understress mechanism and the SST-feedback mechanism. For instance, over a cold cusp (e.g., at 123°W, 3°N and vicinity) the currents coincide in direction with the background south-easterly winds, and hence the stress is less than in a case with no surface current. This adds to the SST-wind feedback effect,

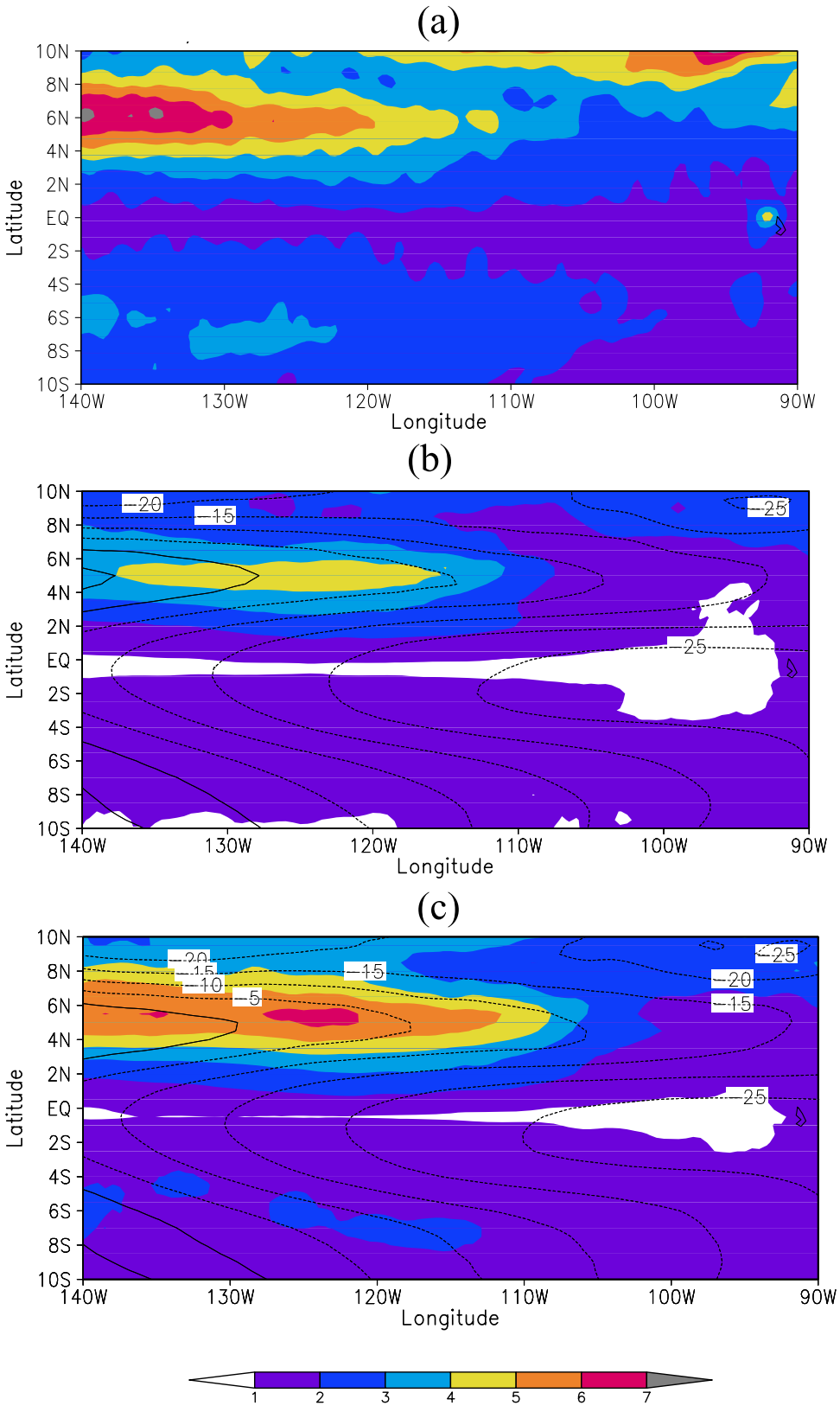

Figure 3. SSH standard deviation due to TIW variability (color, cm). (a) Observations from altimetry. (b) Model Experiment 1, with understress. (c) Experiment 2, no understress. For Figures 3b and 3c, the mean SSH (cm) is added as contours.

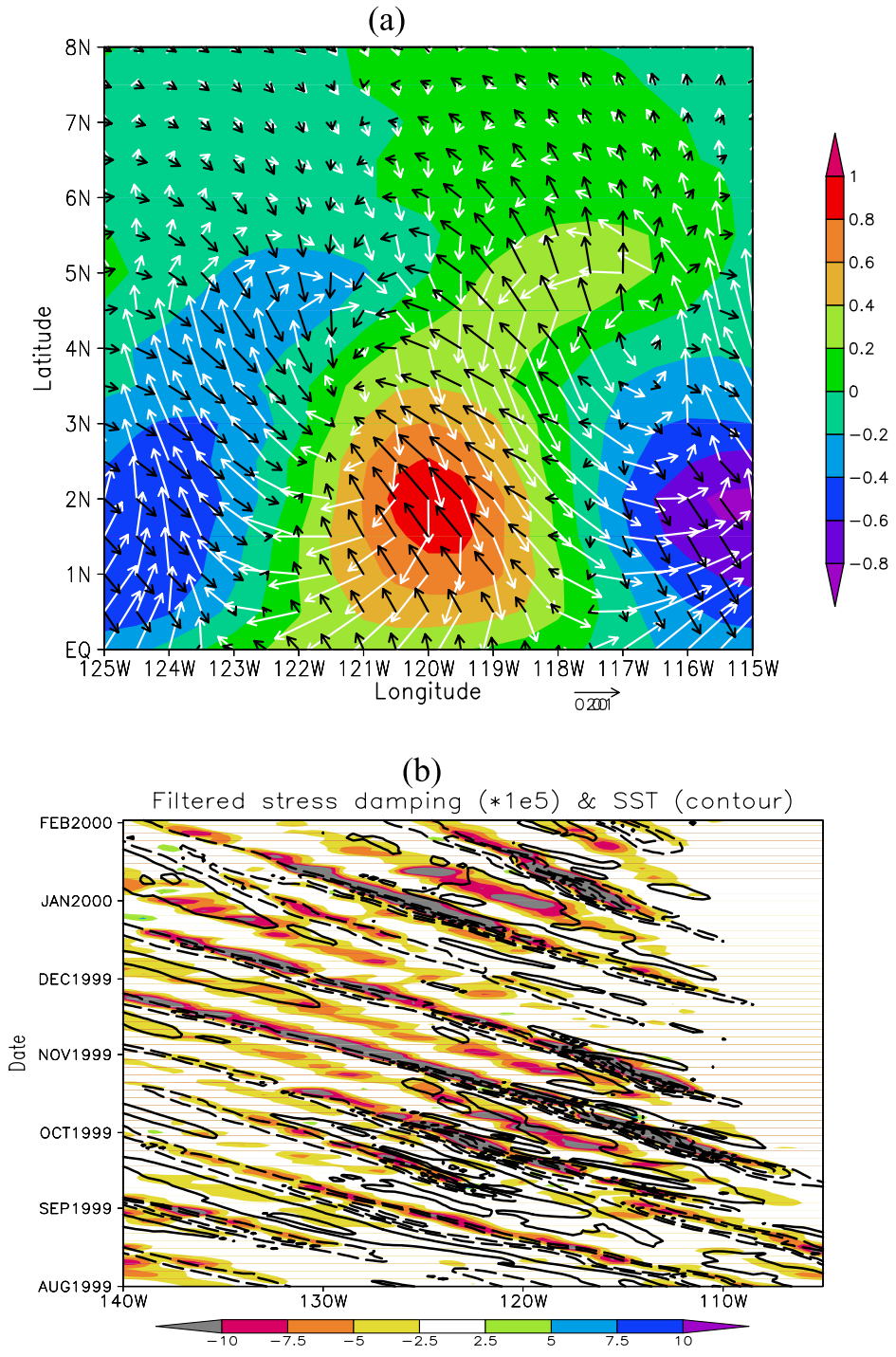

Figure 4. (a) Anomalies of SST (color), surface stress (black vectors), and surface current (white vectors) regressed onto SST at 2°N, 120°W. Units for current and stress are arbitrary. (b) Hovmoller plot of filtered stress damping term (color, units of 10^{-5} kg m s^{-3}) and filtered SST (°C, contoured at 0.5°C intervals, negative dashed, zero omitted) averaged between latitudes 2.5°N and 3.5°N. All from model Experiment 1.

which also leads to reduced stress in the cold cusps, due to the atmospheric boundary layer adjustments (the process discussed by *Seo et al.* [2007]). Consequently there is a negative correlation between the stress anomaly and the current velocity. The stress damping is often largest in the cold cusps of TIWs (as seen from a longitude-time Hovmöller plot, Figure 4b).

[35] The terms in the EKE budget are evaluated first using a value of $h = 95$ m, as in the EKE calculations of section 4.1 (sensitivity to depth average is discussed below). The results for the 1 year time average, averaged in longitude between 140°W and 110°W, for Exp. 1 and Exp. 2, are shown in Figure 5. For the case with understress (Figure 5a), the barotropic conversion term (thick solid line) has a large

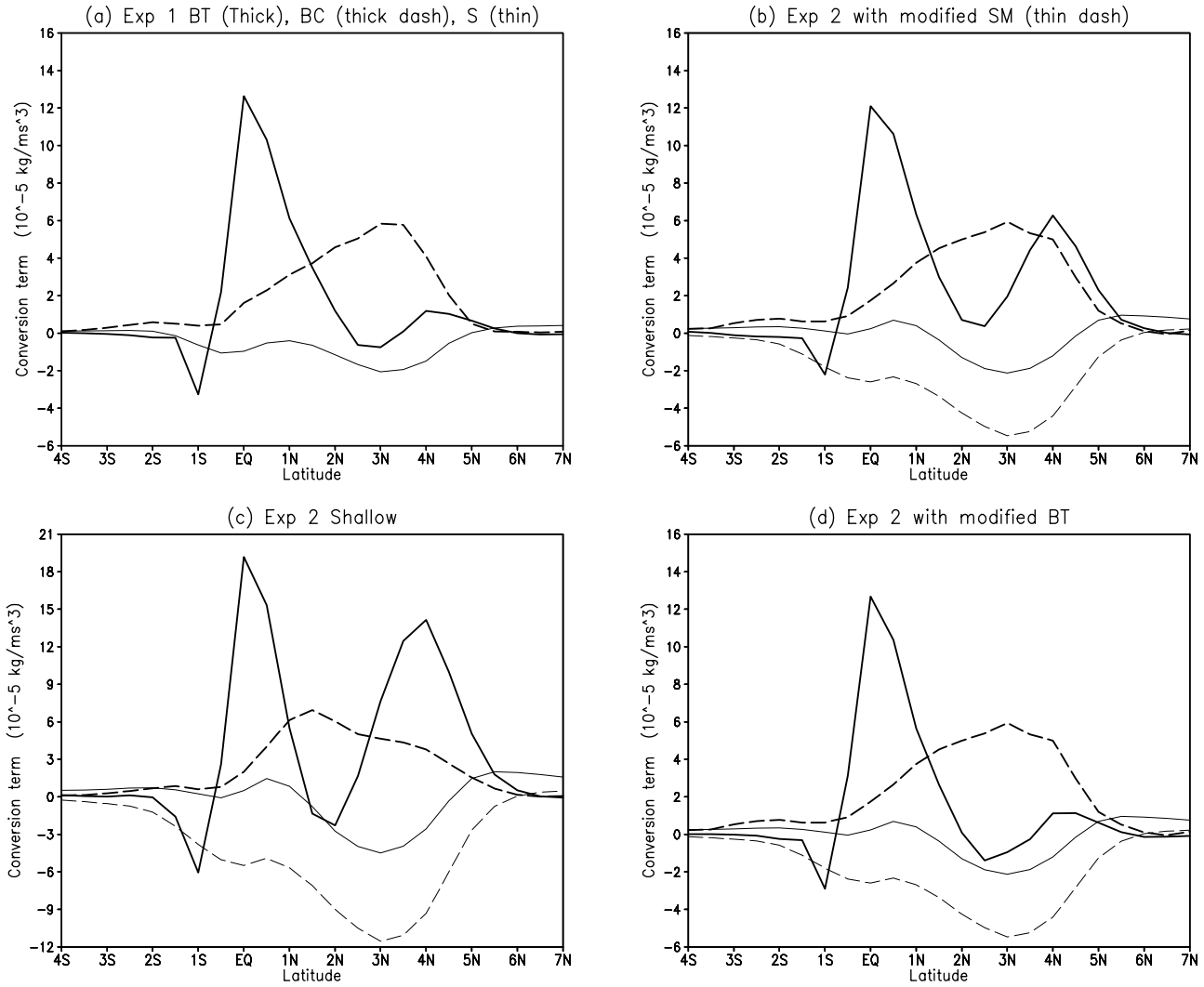

Figure 5. Eddy kinetic energy budget terms, depth average, and longitude average (140°–110°W). Barotropic conversion is marked with a thick solid line, baroclinic conversion with a thick dash, stress-current feedback with thin solid (units of 10^{-5} kg m s^{-3}, equivalent to 10^{-5} J m^{-3} s^{-1}). (a) Experiment 1 (with understress), depth-averaged to 95 m. (b) Experiment 2 (no understress), depth-averaged to 95 m; the modified stress-current feedback is shown as a thin dash. (c) As in Figure 5b, but depth-averaged to 45 m. (d) As in Figure 5b, but using the mean shear from Experiment 2 (no understress) and the eddy part from Experiment 1 (understress) to compute the barotropic term.

magnitude near the equator (due to meridional shear between the EUC and SECN), while the baroclinic conversion term (thick dashes) is significant between the equator and 5°N, peaking at around 3°N (partly due to the near surface temperature front, and partly due to deeper vertical shear of the equatorial currents), while the stress-damping term (thin solid) also has its largest values centered on 3°N, but is rather small compared with the conversion terms. These values are similar in spatial distribution and relative magnitude to those found by *Masina et al.* [1999] for the Pacific Ocean and *Jochum et al.* [2004] and *Seo et al.* [2007] in the Atlantic Ocean. (Note that the three terms shown do not form a closed balance: other important terms include the vertical dissipation of energy in the mixed layer; (M. Jochum, personal communication, 2007) and the radiation term (advection of the pressure anomalies by the eddy currents [*Masina et al.*, 1999]).

[36] When the understress is removed (Exp. 2), a large secondary maximum of the barotropic conversion term occurs near 4°N, (the shear zone between the SECN and NECC), while the peak in baroclinic conversion is slightly changed in location but not in amplitude (Figure 5b). Meanwhile, the stress-damping term (as represented by term S) does not change much between runs (compare thin solid line in Figures 5a, and 5b).

[37] At first glance these results suggest that in the 1-year balance, the difference in EKE between Exp. 1 and Exp. 2 is due to the change in mean current shear at 4°N, (which would influence the barotropic conversion term), while the understress has little impact. However, there is another possibility, which cannot be detected in this balanced result. If the understress has a significant damping effect on the eddy amplitude, it would have two effects on the EKE balance.

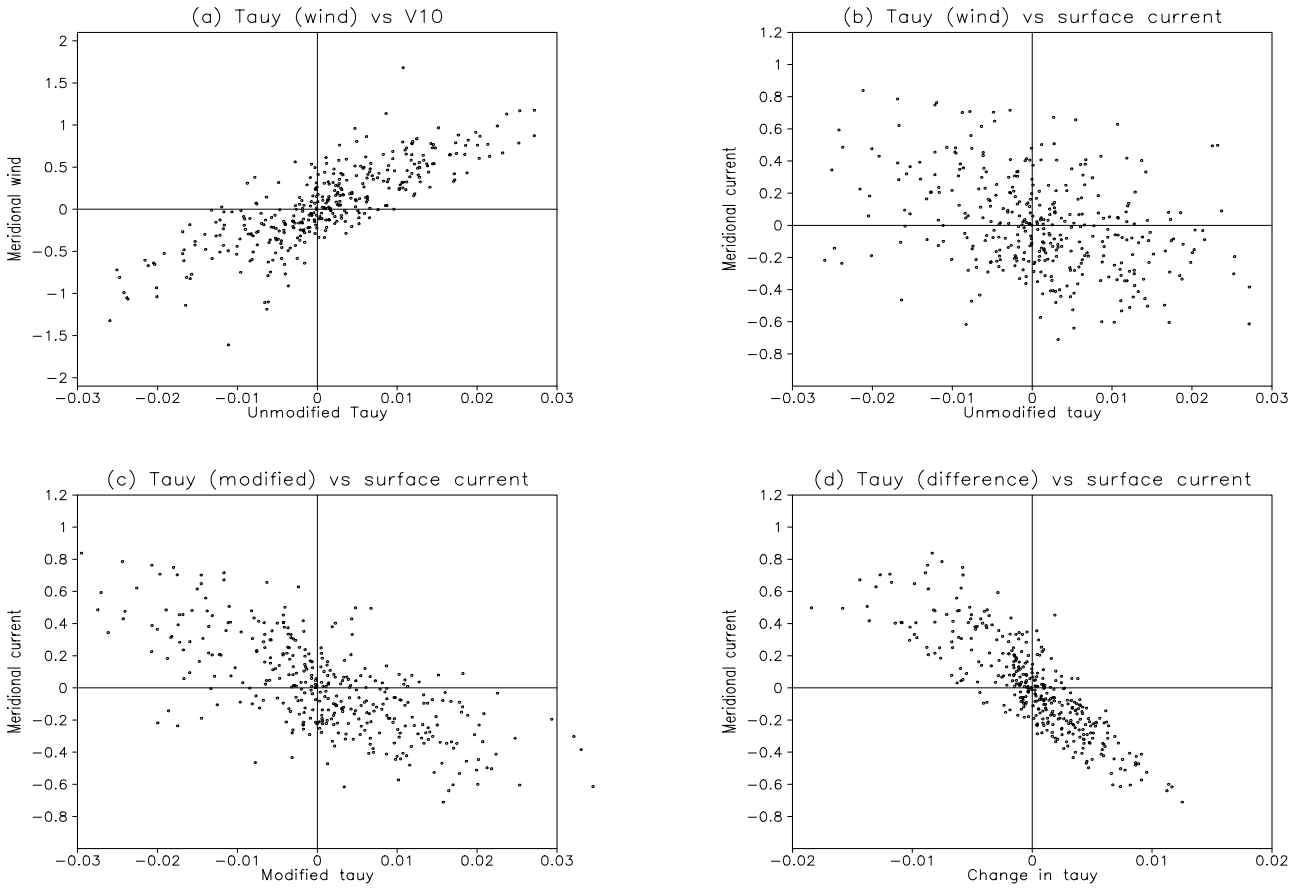

Figure 6. Scatterplots of the meridional component of surface stress τ^y versus wind or current values. All quantities are filtered, and from model Experiment 2. (a) Unmodified stress $\tau_W{}^y$ versus meridional wind. (b) Unmodified stress versus meridional current. (c) The modified stress $\tau_m{}^y$ versus meridional current. (d) The difference between the modified and the unmodified stress versus meridional current. Units of stress are N m^{-2}; wind and currents are in m s^{-1}.

Firstly it would act to reduce the stress-damping term S, and secondly it would affect the barotropic conversion term BT, because these terms are dependent not just on the stress and the mean shear respectively, but also on the eddy part (u′, v′) of the flow (see equation (6)). Thus it is difficult to assess the true importance of the understress from the balanced state.

[38] An alternative approach is to consider the tendency in EKE if the understress effect is suddenly switched on. Here we can take the results from Exp. 2 (where the eddies have not been affected by understress) and compute the correlation of the eddy currents with the stress $\underline{\tau}_m$ that would have been calculated were the surface current taken into account, using

$$\underline{\tau}_m = \frac{\underline{\tau}_W |\underline{U}_{10} - \underline{U}_C| (\underline{U}_{10} - \underline{U}_C)}{|\underline{U}_{10}| \underline{U}_{10}}, \tag{7}$$

where $\underline{\tau}_W$ is the original surface (wind forced) stress in Exp. 2. We have assumed the change of the drag coefficient is small when the relative motion is added (see section 3.3). Thus this approach is an approximate method to gauge the true impact of understress, and it may be noted that it does not include any of the consequences of the modification on the size of the other terms or on the eddy amplitude, which are included in the full model of Exp. 1.

[39] The direct effect of switching on the ocean current influence via equation (7) can be viewed from scatterplots of the filtered stress versus filtered wind or current values (Figure 6). For the no-understress Exp. 2, the stress anomalies $\underline{\tau}_W{}'$ are related to the meridional wind anomalies (Figure 6a), as expected from equations (1) and (2), but show no clear relation to surface current (Figure 6b). These unmodified stress anomalies have a magnitude mostly less than 0.02 N m^{-2}. However, the modified stress values $\underline{\tau}_m{}'$ do show an approximately linear relationship with surface current (Figure 6c). When the difference is taken between the modified and the unmodified stress, $\underline{\tau}_m{}' - \underline{\tau}_W{}'$ (Figure 6d), differences of up to 0.01 N m^{-2} occur when the surface current anomaly is strong (magnitude of 0.5 m s^{-1} or more). In other words, the effect of the eddy surface current on stress can be up to half the total filtered stress value.

[40] When the modified stress (equation (7)) is used, the new stress-damping term is given by

$$S_m = \frac{\left(\underline{u_c}' \bullet \underline{\tau}_m'\right)}{h}, \tag{8}$$

which provides a measure of the magnitude of the damping effect on the eddies *before* the eddies are reduced in amplitude.

Table 1. Estimates of E-folding Time for Experiment 2 at the Equator and at 3°N Using Unmodified and Modified Stress Values

	EKE ($J\ m^{-3}$)	Damping Rate ($J\ m^{-3}\ s^{-1}$)	E-folding Time (days)
Experiment 2 EKE Equator	100	-1×10^{-5}	100
Experiment 2 Equator Modified Stress	100	-2×10^{-5}	50
Experiment 2 at 3°N	60	-2×10^{-5}	30
Experiment 2 at 3°N Modified Stress	60	-5×10^{-5}	12

The resulting modified stress−damping term (S_m) for Exp. 2 is shown on Figure 5b (thin dashed line). It is significantly larger than the unmodified term and is comparable in magnitude to the baroclinic and barotropic conversion terms between 1° and 6°N.

[41] It should be noted here that the importance of the modified stress-damping term is not particularly sensitive to the choice of depth of averaging. For example, when considering an upper ocean budget to 45 m for Experiment 2 (Figure 5c), the BT and S terms become larger in absolute magnitude than for the 95 m case (Figure 5b), while the modified stress-damping term S_m becomes second only in magnitude to that of BT near the equator. For a deeper average to 172 m (well below the core of the strong equatorial zonal jets in this longitude range and in this model), the S_m term is still almost half as much as the BT value near the equator and comparable to the other terms at 4°N (not shown).

[42] The implication of these new results is that the introduction of understress leads to a significant reduction in EKE and to a new balance of terms in the EKE equation. It is thus an important effect in the dissipation of TIW EKE, as will also be shown later from analysis of the Ekman pumping velocity.

[43] From Figures 2 and 5, an estimate of the e-folding timescale implied by the stress term can be derived. Table 1 lists the estimates for near the equator (where the EKE is highest) and at 3°N (where the stress damping is high), for experiment 2. The e-folding times at the equator are 100 days and 50 days using the unmodified and the modified stress term respectively. At 3°N the corresponding decay times are just 30 days and 12 days respectively. Considering that the period of TIWs is just 15−30 days, these decay times would imply a significant reduction in eddy activity and readjustment of the flow if the understress effect were to be turned on, and is consistent with the reduced EKE found in Exp 1.

[44] The question remains as to whether the difference in the barotropic conversion term between the experiments at 4°N (Figures 5a and 5b, thick solid lines) is due to reduced mean shear, or reduced eddy activity, or both. To answer this we start by viewing the long term time-mean of $\partial \underline{U}/\partial y$ (Figure 7, for experiments 1 and 2) which has been identified as the important component of the barotropic conversion term by *Jochum et al.* [2004]. At the surface there is little difference between the two experiments (maximum absolute shear at the surface of $4.16 \times 10^{-6} s^{-1}$ for Exp. 2, $4.06 \times 10^{-6} s^{-1}$ for Exp. 1), while in the thermocline Exp. 1 has slightly larger values (by about 10%). It appears to be counterintuitive to have larger shear in the case of understress, which generally reduces equatorial currents in coarse global models [*Pacanowski*, 1987], but it may be caused either by the reduction of the extraction of energy from the mean by eddies or a nonuniform change of the zonal mean currents. These small differences suggest that the BT term is mainly being modified by eddy current component.

[45] To verify the fact that mean shear was not causing the difference in BT term at 4°N, BT was recomputed for Exp. 2 but taking the mean shear from Exp. 1, and the results (not shown) were essentially unchanged from the full Exp. 2 term seen in Figure 5b. Alternatively, when BT is computed using the mean shear from Exp 2 (no understress), and the eddy part from Exp. 1 (understress), the result is almost identical to that for Exp. 1 alone, as can be seen by comparing Figures 5d and 5a. These results show that the differences in the BT term between Exp. 1 and Exp. 2 is mostly due to the change in eddy amplitude. A physical explanation for these results is that the barotropic conversion in the SECN/NECC shear zone is heavily dependent on the strength of the eddies that are available to extract energy, more so than in the EUC/SECN shear zone where the mean shear appears to determine the conversion term [*Weisburg and Weingartner*, 1988].

[46] In the next two sections we look in detail at the interaction between the ocean and atmosphere on the scale of the TIWs and consider the reason for the decreased EKE when understress is introduced.

5. Modulation of Surface Stress and Ekman Pumping Fields

[47] As discussed in sections 1 and 2, the surface stress curl fields and hence the Ekman pumping may be modified by ocean eddies either by the effect of SST gradients on the overlying wind, or from the understress effect. One technique to examine the relative effects of each process is to regress the filtered stress curl fields onto indices of the TIW activity, for each of the 3 experiments described above. Note that in this section we refer to high pass filtered and regressed fields as anomalies.

5.1. Surface Stress Curl

[48] If we choose the high-pass SST at a particular location along the propagation path of the TIWs as the TIW index (section 3.3), some interesting features are seen in the field of regressed wind stress curl (Figure 8). The observations show large curl anomalies in two distinct latitude ranges: one mostly within 2° of the equator, and one centered on 4°−5°N (Figure 8a). The near-equatorial anomalies are reproduced in all 3 experiments (but with somewhat larger amplitudes in Exp. 3, the atmosphere only simulation, Figure 8d). Here the curl response is governed by the SST-wind feedback (indeed further examination showed that they were linearly dependent on the cross-wind SST gradient, as discussed by *Chelton et al.* [2001]). The higher latitude anomalies (4°−5°N) are

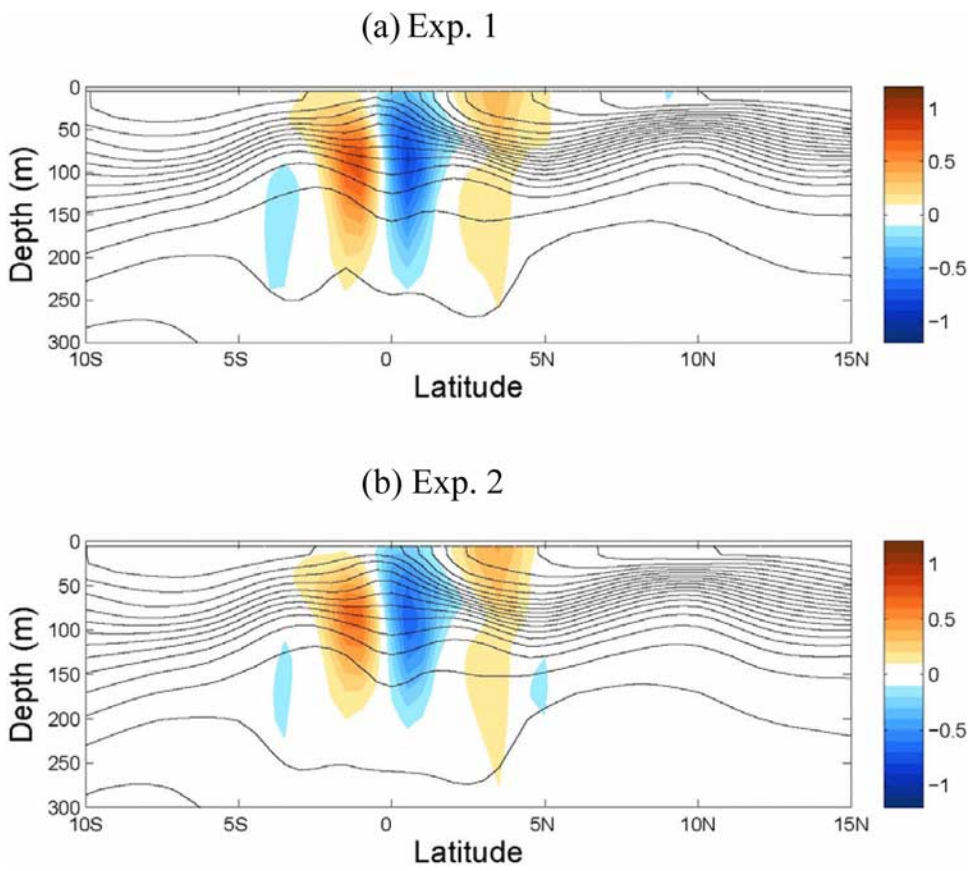

Figure 7. Latitude-depth section of annual mean meridional shear of zonal velocity (color, 10^{-5} s^{-1}), averaged between 110°W and 100°W. Potential density is contoured at 0.25 kg m^{-3} intervals. (a) Model Experiment 1, with understress and (b) Experiment 2, no understress.

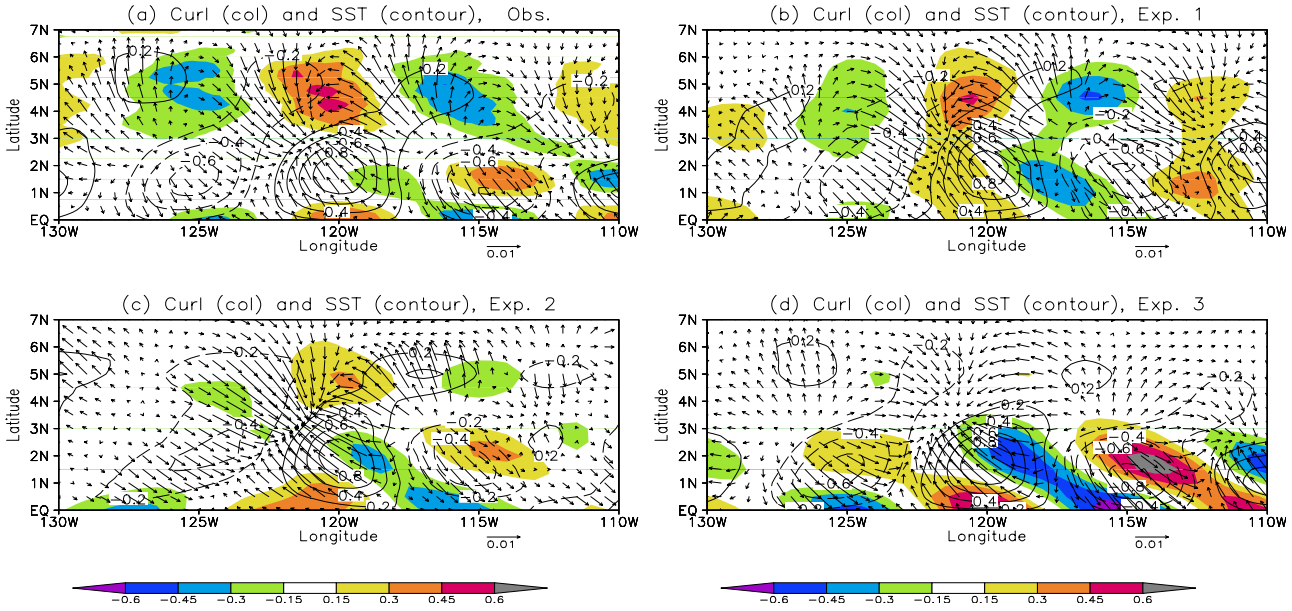

Figure 8. Curl of the anomalous stress (color) regressed onto SST. Units 10^{-7} N m^{-3} K^{-1}. Also shown are SST (contour) and vectors of stress (N m^{-2} K^{-1}, scale arrows at bottom right). (a) Using observations of SST from TMI, and stress derived from QuikSCAT, (b) model Experiment 1, (c) Experiment 2, and (d) Experiment 3.

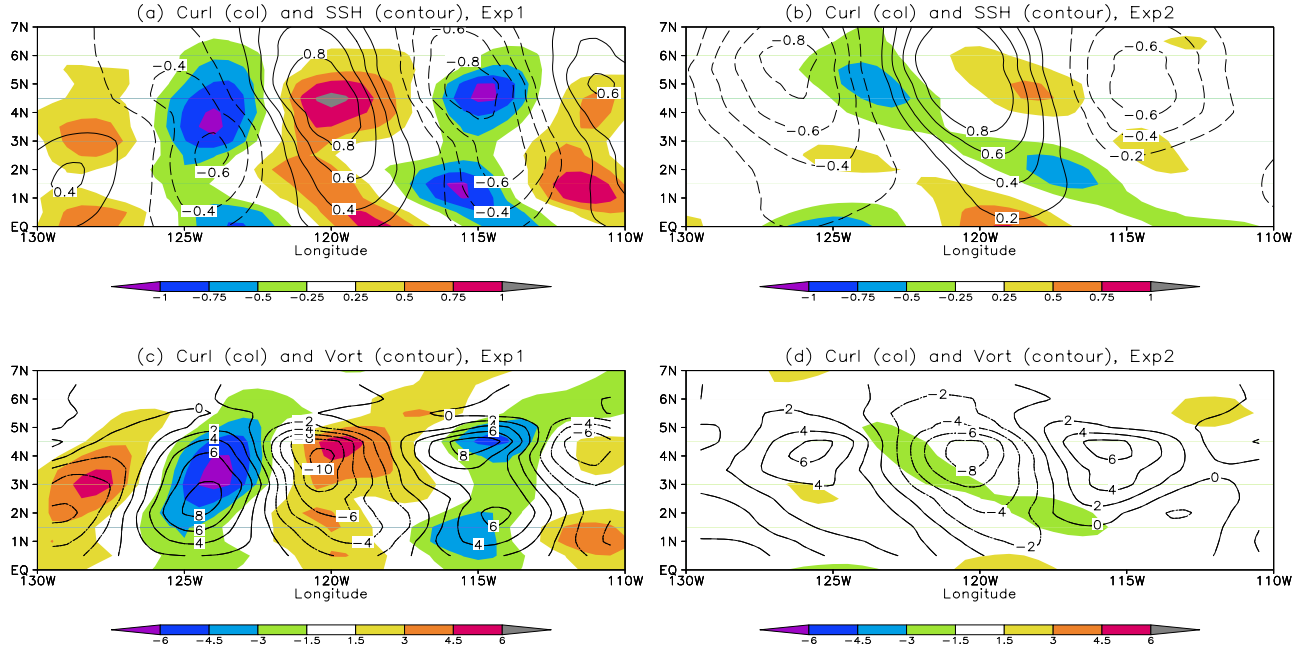

Figure 9. (a) Curl of the anomalous stress (color) regressed onto SSHA at 120°W, 4.5°N, from Experiment 1. Units 10^{-6} N m^{-3} m^{-1} of SSH. The SSH regression is overlaid as contours. (b) As in Figure 9a, but for Experiment 2. (c) Curl of the anomalous relative motion $\underline{U_s}$ (10^{-5} s^{-1} m^{-1}) from Experiment 1 with the ocean vorticity (10^{-5} s^{-1} m^{-1}) regression overlaid as contours. (d) As in Figure 9c, but for Experiment 2.

reproduced in Exp 1 (Figure 8b), when understress is included, but are much weaker in Exp. 2 (Figure 8c) and negligible in Exp. 3 (Figure 8d). At these latitudes we hypothesize that the effect of surface ocean current vorticity on the stress is mainly governing the curl response. These differences between the sensitivity runs are not seen in fields of the regressed surface stress *divergence* (not shown), which is governed by the SST-wind feedback in all cases [*Chelton et al.*, 2001; *Small et al.*, 2003].

[49] The importance of the understress to the surface stress curl is more clearly seen when the fields are regressed onto an index of the TIW dynamic variability, namely the high-pass SSH at a particular location along the propagation path of the TIWs. Figures 9a and 9b show the filtered stress curl regressed onto the filtered SSH at 4.5°N, 120°W. Note that this location is in a region of high SSH variance in both the observations and model (Figure 3, also *Kennan and Flament* [2000] observed the center of TIW vortices to be at a similar latitude). For Exp.1, with understress, there is a nearly in-phase relationship between the anomalous stress curl and the anomalies of ocean SSH (Figure 9a), especially in the latitude range 3°–6°N. In contrast, for the run with no understress (Exp. 2), the relationship between anomalous curl and SSH is weaker, such that it is approximately in quadrature (Figure 9b). In this case, there is a small but nonzero anomalous curl signal because the curl has a small dependence on SST at this latitude, and the SST anomaly is spatially related to the SSH anomaly (via advection of the mean SST gradient by the currents, which are dependent on the gradients of the SSH).

[50] If the surface currents are really dominating the filtered and regressed stress curl in Exp. 1, then we may also expect that the filtered relative surface motion $\underline{U_s}'$ will be dominated by the surface current, (i.e. $\underline{U_s}' = (\underline{U_{10}}' - \underline{U_c}') \sim -\underline{U_c}'$), so that its curl will be equal to minus the filtered surface ocean vorticity (as discussed by *Chelton et al.* [2004]). Here primes denote filtered values. The regional model outputs the relative motion $\underline{U_s}$ and the surface ocean currents in Experiment 1. The curl of the relative motion $\nabla \times \underline{U_s}'$ in Exp. 1 is shown in Figure 9c (color) and indeed it can be seen that it is close in magnitude and opposite in phase to the filtered ocean surface vorticity (Figure 9c, contours). In contrast, the curl of the purely atmospheric quantity $\nabla \times \underline{U_{10}}'$ in Exp. 2 shows no relationship with the ocean vorticity (Figure 9d), confirming our hypothesis that the ocean currents are primarily responsible for the curl signatures in Figure 9c.

5.2. Ekman Pumping

[51] Having identified that the understress is mainly contributing to the anomalous stress curl fields for latitudes 3° to 7°N, we next need to examine how that impacts the ocean. Here the Ekman pumping is computed from the nonfiltered surface stress and then filtered and regressed onto the high pass SSH at 4.5°N, 120°W (Figure 10). The Ekman pumping is not applicable near the equator and only the latitude range 2.5° to 7°N is shown.

[52] For the observations (Figure 10a), Ekman pumping anomalies are located slightly south of, and are of the same sign as, the SSHA anomalies. (The reason for the relative southward location of the Ekman pumping extrema may be appearance of the Coriolis acceleration in the denominator of equation (3)). The Ekman pumping anomalies reach a magnitude of 10^{-6} m s^{-1} cm^{-1}, which for a typical SSH anomaly of 5 cm is equivalent to ~0.5 mday^{-1}.

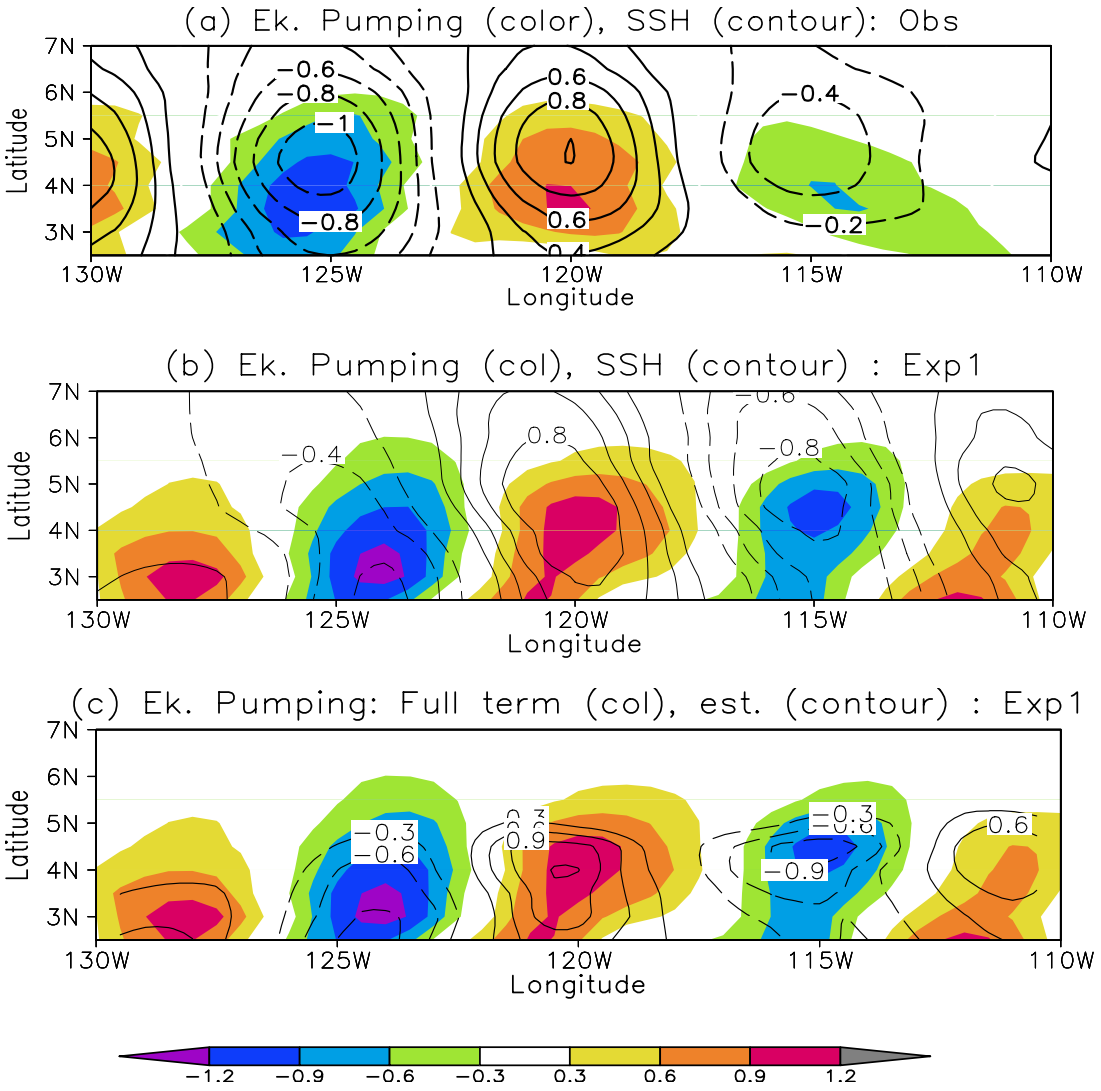

Figure 10. Ekman pumping (color, 10^{-6} m s^{-1} cm^{-1}) and SSHA (contours), both filtered and regressed onto filtered SSHA at 120°W, 4.5°N. (a) Using observations of sea surface height anomalies (SSHA) from TOPEX/POSEIDON altimeters and stress derived from QuikSCAT. (b) As in Figure 10a, but for model Experiment 1. (c) Ekman pumping derived from Experiment 1 stress (color, 10^{-6} m s^{-1} cm^{-1}) and estimated Ekman pumping derived from Experiment 1 vorticity (contours, 10^{-6} m s^{-1} cm^{-1}). Linear regressions onto the filtered SSHA at 4.5°N, 120°W using daily data, 1 September 1999 to 31 October 1999.

[53] According to equation (5) positive (negative) Ekman pumping velocity acts to decrease (increase) the SSHA. The relationships between SSHA and w_E in the TIWs (Figure 10a) indicate that over the SSHA centers the Ekman pumping would act to reduce the SSHA anomaly. We can note a similar relationship in the regional coupled model, Exp. 1 (Figure 10b).

[54] The Ekman pumping derived directly from the surface stress of the model can be compared with that estimated by equation (4b), which assumes a uniform wind and axisymmetric vortex. Using the regressed vorticity values shown in Figure 9c (contours), and a typical mean wind of 7 m s^{-1}, the estimated Ekman pumping using equation (4b) is shown in Figure 10c (contours). It can be seen that the estimate compares well with the full Ekman pumping derived from the model stress (Figure 10c, color). This strongly supports the hypothesis that the anomalous Ekman pumping seen in Experiment 1 is due mainly to ocean surface currents modifying the stress.

[55] The Ekman pumping anomaly that is given by the linear regression is essentially given by $w_e' = E\eta'$ where η' is SSHA and E is a constant. Thus using equation (5) and isolating the time evolution and dissipation (through Ekman pumping) terms we have

$$\frac{\partial \eta'}{\partial t} = -\frac{\rho'}{\rho_0} E\eta' + \ldots. \tag{9}$$

[56] Using equation (9) the approximate damping timescale for the SSH can be derived. For E = 10^{-6}m s^{-1} (from Figure 10), and using typical values of $\rho' = 1$ kg m^{-3} and $\rho_0 =$ 1025 kg m^{-3}, the e-folding timescale is around 115 days.

Noting that a TIW time period is typically 15–30 days [*Lyman et al.*, 2007], this implies significant damping over 4 to 8 time periods, or, equivalently, over about 40° to 80° of longitude. TIWs are known to propagate between 100°W and 160°W [*Contreras*, 2002]; they can also occasionally be seen just west of the Galapagos islands and as far west as the dateline. Hence the effect of "top drag" alone would be sufficient to damp away a TIW before reaching the end of its path. The reason it does not do so is because of continuous amplification along the path through baroclinic and barotropic source terms (section 4).

[57] The estimated decay time of the SSHA under Ekman pumping (115 days) is longer than the EKE damping time computed in section 4.2 (50 days in the "unmodified" scenario). The difference may partly relate to the EKE being a quadratic function of amplitude, so that its e-folding timescale is half of that for amplitude alone.

6. Discussion

[58] The process of top-drag may be added to the more well known damping processes included in ocean models, such as mixing along isopycnal surfaces [*Gent and McWilliams*, 1990], vertical diapycnal mixing [e.g., *Large et al.*, 1994], internal wave mixing [*Jayne and St. Laurent*, 2001], and bottom drag. It is clear that inclusion of the understress effect in a GCM will require some reassessment of the impact of the imposed lateral and vertical mixing on the dynamics and thermodynamics of the ocean model. Further, this assessment should ideally be done in a coupled model due to feedbacks between the ocean and atmosphere system [*Richards et al.*, 2009; hereafter referred to as R2009].

[59] The EKE in the understress experiment is reduced by 10% or more in the latitude range 1°S to 6°N (Figure 2). This includes the range close to the equator where the SST-wind feedback is strong (e.g., south of 3°N, Figure 8d). It is therefore likely that the two feedbacks effects are not mutually exclusive in this region. As the understress effect modifies the surface stress and heat fluxes, the evolving SST field with understress will be different from that without, and hence the magnitude of the stress modulation due to wind-SST feedback will differ between experiments. (This was confirmed by analysis of the differences (Exp. 1 minus Exp. 2) in regressed stress curl near the equator, which were spatially related to differences in the regressed SST, not shown). However, north of 3°N (away from the SST front), the damping of TIWs is almost exclusively due to the understress, (Figures 8 and 9).

[60] Previous modeling studies have shown that TIWs are important to the heat budget of the eastern Equatorial Pacific [*Vialard et al.*, 2001; *Jochum et al.*, 2004; *Jochum and Murtugudde*, 2006; *Menkes et al.*, 2006; *Dutrieux et al.*, 2008]. At the surface, heat advection by the TIWs provides warming in the Equatorial Front region [*Vialard et al.*, 2001; *de Szoeke et al.*, 2007], which acts against and almost balances the advection by the mean flow [*de Szoeke et al.*, 2007; R2009]. The fact that TIW activity is reduced when understress is included suggests that the heat advection by TIWs will also be reduced. This has been confirmed by an analysis of the eastern equatorial Pacific mixed layer heat budget (not shown), following the method of R2009. However, there is a compensating effect in that the reduced overall easterly stress will lead to less upwelling and a weaker westward SEC, which acts to reduce the cooling on and close to the equator. The net effect is that Exp. 1 has a reduction in mean SST (relative to Exp. 2) at latitudes 2°–4°N in most months, peaking in August at about 0.4°C, with slight warming to the north of that, but a small SST difference on the equator, as seen in a monthly mean IROAM 8 year "climatology" of the SST difference (between Exp. 1 and Exp. 2) averaged between120°W and 100°W (Figure 11).

7. Conclusions

[61] In this paper we use a numerical model and satellite observations to show that the inclusion of ocean current in the surface stress (the so-called "understress"), has a significant damping effect on eddies, a process originally predicted theoretically by *Dewar and Flierl* [1987]. It thus adds to the damping caused by modulations of surface stress by atmospheric boundary layer response to SST gradients, and its feedback onto the ocean [*Seo et al.*, 2007]. The results of this paper also show that the surface currents of TIWs need to be known for proper estimation of stress in the eastern Equatorial Pacific.

[62] When the surface current is included in the stress, the Eddy Kinetic Energy of Tropical Instability Waves in the Pacific Ocean is found to reduce by a factor of about 1.5. However, using a standard analysis of the EKE budget, the effect of understress on the damping of TIWs appears to be small. This is because the stress-damping term is dependent on the correlation of the stress anomaly and the current anomaly, so that the damping term diminishes as the eddies, and their currents, weaken. A novel method is applied to the EKE budget to reveal the magnitude of the stress damping term before the eddies have been weakened. This shows that the EKE damping due to understress is comparable in size to the barotropic and baroclinic conversion terms. In the absence of generation and conversion terms, the understress would cause the EKE to decay on an e-folding timescale of just 20–50 days, comparable to the time period of the TIWs.

[63] Reasons for the EKE reduction were explored using regressions of the filtered surface stress fields onto indices of TIW activity, for model and observations. It was found that the curl of the stress is influenced by both SST-wind feedback and understress, but in separate latitude bands. In the band from 3°N to 8°N, the curl of the stress is approximately proportional to the SSHA and the surface ocean vorticity in a fully coupled experiment, but not in the experiment with no understress. These results suggest that the understress is having a significant impact on the stress fields. This modulation of the curl of the stress leads to Ekman pumping anomalies and damping of the TIWs, the so-called "top-drag" effect by *Dewar and Flierl* [1987]. The Ekman pumping anomalies compare well with a rough estimate which assumes that only the understress is modifying the stress. The consequent dissipation has an e-folding timescale of 115 days.

[64] Finally, it is found that the reduction of TIW activity due to understress has an effect on the surface and mixed layer temperatures of the eastern Equatorial Pacific. At the Equatorial Front, a reduction of the heating by eddy advec-

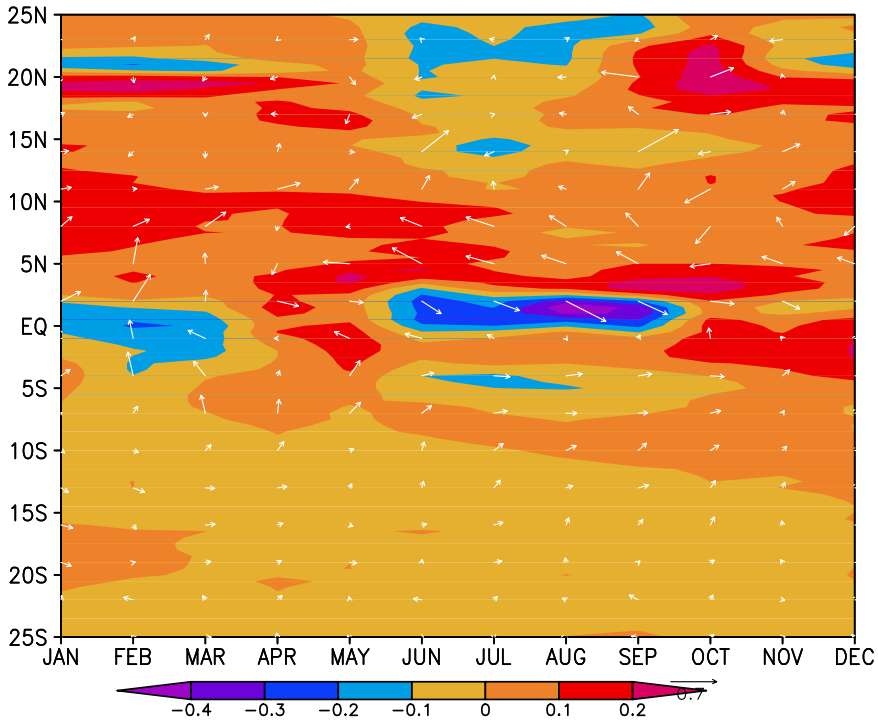

Figure 11. Annual cycle of the difference in monthly mean SST (°C), Experiment 1 minus Experiment 2, as a function of latitude. The data is averaged between 120°W and 100°W. 10-m wind differences are also shown, northward pointing up and eastward pointing right, with a 0.7 m s^{-1} scale arrow shown close to the color bar. From IROAM 8-year climatology.

tion when understress is included leads to a cooler SST (by up to 0.4°C) relative to the case with no understress. However, on the equator, this cooling effect is compensated for by the reduced stress-driven upwelling, so the equatorial SST difference is small.

[65] **Acknowledgments.** Hyodae Seo and Markus Jochum are thanked for useful discussions. We are grateful for the comments of two anonymous reviewers who improved the paper. S.-P.X., K.R., and R.J.S. were supported by NASA grant NAG-10045 and JPL contract 1216010, and the Japan Agency for Marine-Earth Science and Technology (JAMSTEC) through its sponsorship of the International Pacific Research Center. S.-P.X. and R.J.S. were also supported by Japan Ministry of Education, Culture, Science and Technology through the Kyosei-7 Project. IPRC contribution 605 and SOEST contribution 7673.

References

Baturin, N. G., and P. P. Niiler (1997), Effects of instability waves in the mixed layer of the equatorial Pacific, *J. Geophys. Res.*, *102*, 27,771–27,793.

Bye, J. A. T. (1986), Momentum exchange at the sea surface by wind stress and understress, *Quart. J. R. Meteorol. Soc.*, *112*, 501–510.

Chelton, D. B., S. K. Esbensen, M. G. Schlax, N. Thum, M. H. Freilich, F. J. Wentz, C. L. Gentemann, M. J. McPhaden, and P. S. Schopf (2001), Observations of coupling between surface wind stress and sea surface temperature in the Eastern Tropical Pacific, *J. Clim.*, *14*, 1479–1498.

Chelton, D. B., M. G. Schlax, M. H. Freilich, and R. F. Milliff (2004), Satellite measurements reveal persistent small-scale features in ocean winds, *Science*, *303*, 978–983.

Contreras, R. F. (2002), Long-term observations of tropical instability waves, *J. Phys. Oceanogr.*, *32*, 2715–2722.

Cornillon, P., and K.-A. Park (2001), Warm core ring velocities inferred from NSCAT, *Geophys. Res. Lett.*, *28*, 575–578.

Cox, M. D. (1980), Generation and propagation of 30-day waves in a numerical model of the Pacific, *J. Phys. Oceanogr.*, *10*, 1168–1186.

de Szoeke, S. P., S.-P. Xie, T. Miyama, K. J. Richards, and R. J. O. Small (2007), What maintains the SST front north of the eastern Pacific equatorial cold tongue, *J. Clim.*, *20*, 2500–2514.

Dewar, W. K., and G. R. Flierl (1987), Some effects of the wind on rings, *J. Phys. Oceanogr.*, *17*, 1653–1667.

Ducet, N., P. Y. LeTraon, and G. Reverdin (2000), Global high resolution mapping of ocean circulation from TOPEX/Poseidon and ERS-1 and 2, *J. Geophys. Res.*, *105*, 19,477–19,498.

Dutrieux, P., C. E. R. Menkes, J. G. Vialard, P. Flament, and B. Blanke (2008), Lagrangian study of tropical instability vortices in the Atlantic, *J. Phys. Oceanogr.*, *38*, 400–417.

Fairall, C. W., E. F. Bradley, D. P. Rogers, J. B. Edson, and G. S. Young (2003), Bulk parameterization on air-sea fluxes: Updates and verification for the COARE algorithm, *J. Clim.*, *16*, 571–591.

Gent, P. R., and J. C. McWilliams (1990), Isopycnal mixing in ocean circulation models, *J. Phys. Oceanogr.*, *20*, 150–155.

Hashizume, H., S.-P. Xie, W. T. Liu, and K. Takeuchi (2001), Local and remote response to tropical instability waves: A global view from space, *J. Geophys. Res.*, *106*, 10,173–10,185.

Hayes, S. P., M. J. McPhaden, and J. M. Wallace (1989), The influence of sea surface temperature on surface wind in the eastern equatorial Pacific: Weekly to monthly variability, *J. Clim.*, *2*, 1500–1506.

Jayne, S. R., and L. St. Laurent (2001), Parameterizing tidal dissipation over rough topography, *Geophys. Res. Lett.*, *28*, 811–814.

Jochum, M., P. Malanotte-Rizzoli, and A. Busalacchi (2004), Tropical instability waves in the Atlantic Ocean, *Ocean Mod.*, *7*, 145–163.

Jochum, M., and R. Murtugudde (2006), Temperature advection by tropical instability waves, *J. Phys. Oceanogr.*, *36*, 592–605.

Jochum, M., C. Deser, and A. Philips (2007), Tropical atmospheric variability forced by oceanic interannual variability, *J. Clim.*, *20*, 765–771.

Johannessen, J. A., R. A. Shuchman, G. Digranes, D. R. Lyzenga, C. Wackerman, O. M. Johannessen, and P. W. Vachon (1996), Coastal ocean fronts and eddies imaged with ERS 1 synthetic aperture radar, *J. Geophys. Res.*, *101*, 6651–6667.

Kalnay, E., et al. (1996), The NCEP/NCAR 40-year reanalysis project, *Bull. Amer. Meteorol. Soc.*, *77*, 437–472.

Kelly, K. A., S. Dickinson, M. J. McPhaden, and G. C. Johnson (2001), Ocean currents evident in satellite wind data, *Geophys. Res. Lett.*, *28*, 2469–2472.

Kennan, S. C., and P. J. Flament (2000), Observations of a tropical instability vortex, *J. Phys. Oceanogr.*, *30*, 2277–2301.
Large, W. G., and S. Pond (1981), Open ocean momentum flux measurements in moderate to strong winds, *J. Phys. Oceanogr.*, *11*, 324–336.
Large, W. G., J. C. Mc Williams, and S. C. Doney (1994), Oceanic vertical mixing: A review and a model with a nonlocal boundary layer parameterization, *Rev. Geophys.*, *32*, 363–403.
Levitus, S. (1982), *Climatological Atlas of the World Ocean*, *NOAA Prof. Paper*, vol. 13, 173 pp., U.S. Govt. Printing Office.
Liu, W. T., X. Xie, P. S. Polito, S.-P. Xie, and H. Hashizume (2000), Atmospheric manifestation of tropical instability wave observed by QuikSCAT and Tropical Rain Measuring Mission, *Geophys. Res. Lett.*, *27*, 2545–2548.
Luo, J.-J., S. Masson, E. Roeckner, G. Madec, and T. Yamagata (2005), Reducing climatological bias in an Ocean-Atmosphere CGCM with improved coupling physics, *J. Clim.*, *18*, 2344–2360.
Luther, D. S., and E. S. Johnson (1990), Eddy energetic in the upper equatorial Pacific during the Hawaii to Tahiti shuttle experiment, *J. Phys. Oceanogr.*, *20*, 913–944.
Lyman, J. M., G. C. Johnson, and W. S. Kessler (2007), Distinct 17 day and 33 day tropical instability waves in subsurface observations, *J. Phys. Oceanogr.*, *37*, 855–872.
Martin, A. P., and K. J. Richards (2001), Mechanisms for vertical nutrient transport within a North Atlantic mesoscale eddy, *Deep-Sea Res. II*, *48*, 757–773.
Masina, S., S. G. H. Philander, and A. B. G. Bush (1999), An analysis of tropical instability waves in a numerical model of the Pacific Ocean: 2. Generation and energetics of the waves, *J. Geophys. Res.*, *104*, 29,637–29,661.
McCreary, J. P., and Z. Yu (1992), Equatorial dynamics in a 2.5 layer model, *Prog. Oceanogr.*, *29*, 61–132.
McGillicuddy, D. J., et al. (2007), Eddy/wind interactions stimulate extraordinary mid-ocean plankton blooms, *Science*, *316*, 1021–1026.
Menkes, C. E., et al. (2002), A whirling ecosystem in the equatorial Atlantic, *Geophys. Res. Lett.*, *29*(11), 1553, doi:10.1029/2001GL014576.
Menkes, C. E. R., J. G. Vialard, S. C. Kennan, J.-P. Boulanger, and G. V. Madec (2006), A modeling study of the impact of tropical instability waves on the heat budget of the eastern Equatorial Pacific, *J. Phys. Oceanogr.*, *36*, 847–865.
O'Neill, L. W., D. B. Chelton, S. K. Esbensen, and F. J. Wentz (2005), High-resolution satellite measurements of the atmospheric boundary layer response to SST variations along the Agulhas Return Current, *J. Clim.*, *18*, 2706–2723.
Pacanowski, R. C. (1987), Effect of equatorial currents on surface stress, *J. Phys. Oceanogr.*, *17*, 833–838.
Pacanowski, R. C., and S. M. Griffies (2000), The MOM3 manual, *GFDL Ocean Group Tech. Rep. 4*, 680 pp., Geophysical Fluid Dynamics Laboratory, Princeton, N. J. (Available at http://www.gfdl.noaa.gov/~smg/MOM/web/guide_parent/guide_parent.html)
Pacanowski, R. C., and S. G. H. Philander (1981), Parameterization of vertical mixing in numerical models of tropical oceans, *J. Phys. Oceanogr.*, *11*, 1443–1451.
Park, K.-A., P. C. Cornillon, and D. L. Codiga (2006), Modification of surface winds near ocean fronts: Effects of Gulf Stream rings on scatterometer (QuikSCAT, NSCAT) wind observations, *J. Geophys. Res.*, *111*, C03021, doi:10.1029/2005JC003016.
Pezzi, L. P., J. Vialard, K. J. Richards, C. Menkes, and D. Anderson (2004), Influence of ocean-atmosphere coupling on the properties of tropical instability waves, *Geophys. Res. Lett.*, *31*, L16306, doi:10.1029/2004GL019995.
Philander, S. G. H. (1978), Instabilities of zonal equatorial currents: 2, *J. Geophys. Res.*, *83*, 3679–3682.
Polito, P. S., J. P. Ryan, W. T. Liu, and F. P. Chavez (2001), Oceanic and atmospheric anomalies of tropical instability waves, *Geophys. Res. Lett.*, *28*, 2233–2236.
Qiao, L., and R. H. Weisburg (1998), Tropical instability wave energetics: Observations from the Tropical Instability Wave Experiment, *J. Phys. Oceanogr.*, *28*, 345–360.
Richards, K., S.-P. Xie, and T. Miyama (2009), Vertical mixing in the ocean and its impact on the coupled ocean/atmosphere system in the eastern Tropical Pacific, *J. Clim.*, in press.
Seo, H., M. Jochum, R. Murtugudde, A. J. Miller, and J. O. Roads (2007), Feedback of tropical instability wave-induced atmospheric variability onto the ocean, *J. Clim.*, *20*, 5842–5855.
Small, R. J., S.-P. Xie, and Y. Wang (2003), Numerical simulation of atmospheric response to pacific tropical instability waves, *J. Clim.*, *16*, 3723–3741.
Small, R. J., S. P. de Szoeke, S. P. Xie, L. O'Neill, H. Seo, Q. Song, P. Cornillon, M. Spall, and S. Minobe (2008), Air-sea interaction over ocean fronts and eddies, *Dyn. Atmos. Oceans*, *45*, 274–319, doi:10.1016/j.dynatmoce.2008.01.001.
Song, Q., P. Cornillon, and T. Hara (2006), Surface wind response to oceanic fronts, *J. Geophys. Res.*, *111*, C12006, doi:10.1029/2006JC003680.
Spall, M. A. (2007), Effect of sea surface temperature-wind stress coupling on baroclinic instability in the ocean, *J. Phys. Oceanogr.*, *37*, 1092–1097.
Vialard, J., C. Menkes, J.-P. Boulanger, P. Delecluse, E. Guilyardi, M. J. McPhaden, and G. Madec (2001), A model study of oceanic mechanisms affecting Equatorial Pacific sea surface temperatures during the 1997–98 El Nino, *J. Phys. Oceanogr.*, *31*, 1649–1675.
Wang, Y. (2001), An explicit simulation of tropical cyclones with a triply-nested movable mesh primitive equation model-TCM3. part I: Model description and control experiment, *Mon. Weather Rev.*, *129*, 1370–1394.
Wang, Y., S.-P. Xie, H. Xu, and B. Wang (2004), Regional model simulations of marine boundary layer clouds over the Southeast Pacific off South America. part I: Control experiment, *Mon. Weather Rev.*, *132*, 274–296.
Weisburg, R. H., and T. J. Weingartner (1988), Instability waves in the Equatorial Atlantic Ocean, *J. Phys. Oceanogr.*, *18*, 1641–1657.
Wentz, F. J., and D. K. Smith (1999), A model function for the ocean-normalised radar cross-section at 14 GHz derived from NSCAT observations, *J. Geophys. Res.*, *104*, 11,499–11,514.
Wentz, F. J., C. Gentemann, D. Smith, and D. Chelton (2000), Satellite measurements of sea surface temperature through clouds, *Science*, *288*, 847–850.
White, W. B., and J. L. Annis (2003), Coupling of extratropical mesoscale eddies in the ocean to westerly winds in the atmospheric boundary layer, *J. Phys. Oceanogr.*, *33*, 1095–1107.
Xie, S.-P. (2004), Satellite observations of cool ocean-atmosphere interaction, *Bull. Am. Meteorol. Soc.*, *85*, 195–208.
Xie, S.-P., M. Ishiwatari, H. Hashizume, and K. Takeuchi (1998), Coupled ocean-atmospheric waves on the equatorial front, *Geophys. Res. Lett.*, *25*, 3863–3866.
Xie, S.-P., T. Miyama, Y. Wang, H. Xu, S. P. de Szoeke, R. J. O. Small, K. J. Richards, T. Mochizuki, and T. Awaji (2007), A regional ocean-atmosphere model for eastern Pacific climate: Towards reducing tropical biases, *J. Clim.*, *20*, 1504–1522.
Yoder, J. A., S. G. Ackleson, R. T. Barber, P. Flament, and W. M. Balch (1994), A line in the sea, *Nature*, *371*, 689–692.
Zhang, R.-H., and A. J. Busalacchi (2008), Rectified effects of tropical instability wave induced atmospheric wind feedback in the tropical Pacific, *Geophys. Res. Lett.*, *35*, L05608, doi:10.1029/2007GL033028.

P. Dutrieux, Department of Oceanography, School of Ocean and Earth Science and Technology, University of Hawaii, Honolulu, HI 96822, USA.
T. Miyama, Frontier Research for Global Change, Japan Agency for Marine-Earth Science and Technology, 3173-25 Showamachi, Kanazawa-ku, Yokohama, Kanagawa 236-0001, Japan.
K. J. Richards and S.-P. Xie, International Pacific Research Center, University of Hawaii, Post 401, 1680 East-West Road, Honolulu, HI 96822, USA.
R. J. Small, Naval Research Laboratory, Code 7320, Building 1009, Stennis Space Center, MS 39529, USA. (small.ctr.uk@nrlssc.navy.mil)